

Kinetics of the Reactions of Isoprene-Derived Hydroxynitrates: Gas Phase Epoxide Formation and Solution Phase Hydrolysis

M. I. Jacobs, W. J. Burke, and M. J. Elrod

Department of Chemistry and Biochemistry, Oberlin College, Oberlin, Ohio, USA

Correspondence to: M. J. Elrod (mjelrod@oberlin.edu)

Abstract

Isoprene, the most abundant non-methane volatile organic compound (VOC) emitted into the atmosphere, is known to undergo gas phase oxidation to form eight different hydroxynitrate isomers in “high NO_x ” environments. These hydroxynitrates are known to affect the global and regional formation of ozone and secondary organic aerosol (SOA), as well as affect the distribution of nitrogen. In the present study, we have synthesized three of the eight possible hydroxynitrates: 4-hydroxy-3-nitroxy isoprene (4,3-HNI) and E/Z-1-hydroxy-4-nitroxy isoprene (1,4-HNI). Oxidation of the 4,3-HNI isomer by the OH radical was monitored using a flow tube chemical ionization mass spectrometer (FT-CIMS), and its OH rate constant was determined to be $(3.64 \pm 0.41) \times 10^{-11} \text{ cm}^3 \text{ molecule}^{-1} \text{ s}^{-1}$. The products of 4,3-HNI oxidation were monitored, and a mechanism to explain the products was developed. An isoprene epoxide (IEPOX)—a species important in SOA chemistry and thought to originate only from “low NO_x ” isoprene oxidation—was found as a minor, but significant product. Additionally, hydrolysis kinetics of the three synthesized isomers were monitored with NMR. The bulk, neutral solution hydrolysis rate constants for 4,3-HNI and the 1,4-HNI isomers were $(1.59 \pm 0.03) \times 10^{-5} \text{ s}^{-1}$ and $(6.76 \pm 0.09) \times 10^{-3} \text{ s}^{-1}$, respectively. The hydrolysis reactions of each isomer were found to be general acid-catalyzed. The reaction pathways, product yields and atmospheric implications for both the gas phase and aerosol-phase reactions are discussed.

1 **1 Introduction**

2 Isoprene (2-methyl-1,3-butadiene) is a volatile alkene produced mainly by deciduous trees and
3 shrubs whose global emissions have been estimated at 600 Tg yr^{-1} (Guenther et al., 2006),
4 making it the most abundant non-methane volatile organic compound (VOC) in the atmosphere.
5 Because of its abundance and two double bonds (which make it particularly susceptible to
6 oxidation by species such as the OH radical or ozone), isoprene oxidation is important both in the
7 formation of ozone and secondary organic aerosols (SOA) (Carlton et al., 2009).

8 Hydroxynitrates are produced from isoprene oxidation in “high NO_x ” environments (Lockwood
9 et al., 2010; Paulot et al., 2009a). Organic nitrates are products of the reaction between
10 peroxyradicals (ROO) and nitric oxide (NO), and their formation is highly dependent on the alkyl
11 chain length (Atkinson, 1990). The total (non-isomer specific) yield of the isoprene-derived
12 hydroxynitrates has been measured several times, and the measurements span a very large range
13 (from 4.4% to 15%) (Chen et al., 1998; Chuong and Stevens, 2002; Patchen et al., 2007; Paulot
14 et al., 2009a; Sprengnether et al., 2002). Because the formation of the hydroxynitrates results in
15 the sequestration of NO_x , the large variation in the estimated yields of hydroxynitrates has
16 profound implications to the assessments of ozone production caused by isoprene photooxidation
17 (Fiore et al., 2005; Horowitz et al., 2007; von Kuhlmann et al., 2004). The eight possible isomers
18 of isoprene-derived hydroxynitrates and their estimated relative yields (Paulot et al., 2009a) are
19 given in Table 1.

20 The ability of the hydroxynitrates to sequester NO_x depends on the details of their atmospheric
21 fate. The production of organic nitrates creates compounds with a lower vapor pressure that are
22 more hydrophilic than their precursor volatile organic compounds. Thus, organic nitrates are
23 believed to play an important role in SOA chemistry. Ambient aerosol measurements have
24 indicated that 17-23% of molecules in organic aerosol contain the RONO_2 functional group
25 (Rollins et al., 2013). Laboratory studies have indicated that tertiary organic nitrates undergo fast
26 hydrolysis under typical aerosol conditions (Darer et al., 2011; Hu et al., 2011). Recent studies
27 have shown that the partitioning of hydroxynitrates into the particle phase is strongly dependent
28 on the relative humidity; at high RH, α -pinene-derived hydroxynitrates and their hydrolysis
29 products have been observed in SOA (Rindelaub et al., 2014). Uptake into SOA represents a

1 permanent sequestration of NO_x from the gas phase, which leads to a decrease in ozone
2 production associated with hydroxynitrates.

3 However, further gas phase oxidation of hydroxynitrates is possible, and depending on the rate of
4 OH reaction and the product formation mechanism, they may recycle NO_x back into the gas
5 phase. A previous chamber study that investigated the oxidation of isoprene in a “high NO_x ”
6 environment predicted that 60-70% of all hydroxynitrates release NO_x when further oxidized by
7 the OH radical (Paulot et al., 2009a). If the gas phase oxidation is slow and occurs on a long
8 enough time scale, hydroxynitrates may be transported significant distances from the source
9 region to a remote location where the subsequent recycling of NO_x can result in accelerated
10 photochemistry and enhanced ozone formation (Paulot et al., 2012). Understanding how the
11 isoprene-derived hydroxynitrates might react in both the aerosol phase—leading to permanent
12 NO_x sequestration—and gas phase—which could lead to the release of NO_x into the gas phase—
13 is important for the refinement of air quality models.

14 In the present research, we have synthesized some of the isoprene-derived hydroxynitrates to
15 study their possible atmospheric fates: gas phase oxidation and aerosol phase uptake. Three
16 isoprene-derived hydroxynitrates—4-hydroxy-3-nitroxy isoprene (4,3-HNI) and E/Z 1-hydroxy-
17 4-nitroxy isoprene (E/Z 1,4-HNI)—have been synthesized. The OH radical rate constant for 4,3-
18 HNI oxidation has been measured using our lab's flow tube chemical ionization mass
19 spectrometer (FT-CIMS), and a mechanism to explain the observed products has been proposed.
20 Additionally, the hydrolysis rate constants in neutral, bulk aqueous solution have been measured
21 using NMR as the analytical technique. The oxidation and hydrolysis kinetics of a similar,
22 unsaturated hydroxynitrate (1-hydroxy-2-nitroxy-3-butene (1,2-HNB)) were also investigated in
23 order to explore the generality of mechanisms gleaned from similar study of the isoprene-derived
24 species.

25

26 **2 Experimental**

27 **2.1 Synthesis of Hydroxynitrates**

28 The methods used in the syntheses of 4,3-HNI, E/Z 1,4-HNI and 1-hydroxy-2-nitroxy-3-butene
29 (1,2-HNB) are given in the Supplemental Information (SI) section.

1 **2.2 NMR technique**

2 Hydroxynitrate hydrolysis was studied using an NMR-based technique previously developed in
3 our lab (Darer et al., 2011). Hydrolysis of the various hydroxynitrate species was monitored
4 using ^1H NMR (8 scans, 30 s). Chemical shifts were calibrated relative to the solvent HDO peak
5 (4.79 ppm) for all ^1H spectra. The kinetics spectra were collected in aqueous solutions prepared
6 from 99.9% D_2O (Cambridge Isotope Lab, Inc.) and 68 wt % DClO_4 (Sigma-Aldrich).

7 **2.3 Hydroxynitrate hydrolysis experiments**

8 Hydrolysis kinetics measurements were made by collecting sequential ^1H NMR spectra over the
9 course of the hydrolysis experiment (times varied for different isomers) and measuring the
10 depletion of the hydroxynitrates. Each measurement was performed in the same manner: 10 μL
11 of hydroxynitrate were added to a 1-mL aliquot of the desired aqueous solution, and the solution
12 was stirred in a 10-mL beaker. After approximately 1 min of stirring to ensure solution
13 homogeneity, the entire reaction mixture was loaded into an NMR tube, and spectral collection
14 was started. For 1,4-HNI, the relative 1,4-HNI concentration was determined by comparing the
15 nitrate proton peak (5.00 ppm) relative to an internal standard (2,2-dimethyl-2-silapentane-5-
16 sulfonate sodium salt, DSS, which had a nine proton peak at 0.00 ppm). For 4,3-HNI, the
17 relative 4,3-HNI concentration was determined by comparing the 4,3-HNI methyl group protons
18 (1.81 ppm) to the product methyl group protons (1.64, 1.69 and 1.71 ppm). For 1,2-HNB, the
19 relative 1,2-HNB concentration was determined by comparing the 1,2-HNB alcohol group
20 protons (3.8 ppm) to the equivalent product alcohol group protons (3.54 ppm). A first order
21 decay rate law was found to fit the organic hydroxynitrate concentration vs. time data, and the
22 first order rate constants (and thus the lifetimes) of the species were determined.

23 **2.4 HNI gas phase oxidation experiments**

24 **2.4.1 Flow tube apparatus**

25 A schematic of the flow tube apparatus is given in Figure 1 and is similar to the instrument
26 configuration used in a previous study of the OH reaction with isoprene-derived epoxides (Jacobs
27 et al., 2013). The main flow tube was 100 cm in length and constructed with 2.2 cm inner

1 diameter Pyrex tubing. A large flow of O₂ carrier gas (15 STP L min⁻¹) was injected at the rear of
2 the flow tube and served as the bulk flow. The gases necessary to generate the OH radicals were
3 introduced through a 20-cm long, 1.25 cm inner diameter sidearm. The organic hydroxynitrate
4 compounds—which were added by flowing He gas through traps containing the liquid phase of
5 the various species because of their low vapor pressures—and the competitor species
6 (compounds used in the relative determination of OH reaction rate constants) were introduced
7 together through a moveable injector with a fan-shaped Teflon device placed at the end to
8 enhance mixing. All gas flow rates were monitored using calibrated mass flow meters. The
9 ²¹⁰Po α-emitting ionization source was placed between the flow tube and the inlet to the CIMS.
10 O₂ gas (99.99%) at a flow of 6.5 STP L min⁻¹ was passed through the ²¹⁰Po α-emitting ionization
11 source to produce reagent ions. Pressure in the flow tube was monitored using a 0-1000 Torr
12 capacitance manometer, while temperature was measured with Cu-constantan thermocouples and
13 held at 298 ± 2 K for most of the experiments. Most of the flow tube gases were removed at the
14 CIMS inlet using a 31-L s⁻¹ roughing pump. The pressure in the flow tube apparatus was
15 controlled by adjusting the roughing pump valve opening.

16 **2.4.2 OH source**

17 For the present study, OH radicals were prepared by passing a dilute mixture of carbon
18 tetrafluoride (CF₄) in He through a microwave discharge produced by a Beenakker cavity
19 operating at 50 W. This microwave discharge-initiated dissociation of CF₄, followed by reaction
20 with H₂O leads to the production of OH radicals:



23 The dilute CF₄ mixture was created by combining 4% CF₄/ He (0.50 STP mL min⁻¹) with a flow
24 of He (99.999%, 5.00 STP L min⁻¹). This mixture was flowed through the Beenakker cavity to
25 produce fluorine atoms (Reaction 1). The fluorine atoms were then injected in the flow tube side
26 arm and mixed with H₂O (produced by bubbling 12 mL min⁻¹ He through a trap filled with H₂O)
27 to produce OH radicals (Reaction 2). Because H₂O is in great excess in the side arm ([H₂O] ~ 2 x
28 10¹⁴ molecules cm⁻³) and Reaction 2 is very fast (1.4 x 10⁻¹¹ cm³ molecule⁻¹ s⁻¹) (Atkinson et al.,
29 2007), the OH-producing reaction has a very short lifetime of about 0.4 ms, ensuring all fluorine

1 atoms are quickly consumed. For similar experimental conditions, we have estimated that this
2 source leads to a maximum OH radical concentration of $\sim 5 \times 10^{11}$ molecules cm^{-3} (Elrod, 2011).

3 **2.4.3 CIMS detection**

4 The chemical ionization reagent ions in this study were produced using a commercial ^{210}Po α -
5 emitting source consisting of a hollow, cylindrical (69 x 12.7 mm) aluminium body with 10 mCi
6 (3.7×10^8 disintegrations s^{-1}) of ^{210}Po coated on the interior walls. All oxygenated organic
7 species were detected using a proton transfer CIMS (PTR-CIMS) scheme. Protonated water
8 clusters were used as the reagent ion to transfer a proton to the oxygenated acceptor, M:



10 The $\text{H}^+(\text{H}_2\text{O})_n$ ions were produced by passing a large O_2 flow ($6.5 \text{ STP L min}^{-1}$) through the
11 ionization source with H_2O impurities being sufficiently abundant to produce an adequate amount
12 of reagent ions. The dominant chemical reagent ion was $\text{H}^+(\text{H}_2\text{O})_4$, and the predominant proton
13 transfer species detected were the protonated (and partially hydrated) analogues of the neutral
14 precursor oxygenated compound. For both the OH rate constant and product studies, all ions
15 ($\text{MH}^+(\text{H}_2\text{O})_n$) assigned to a particular species (M) were summed and normalized to the total
16 reagent ion signal ($\text{H}^+(\text{H}_2\text{O})_n$) for that particular experiment in order to determine a CIMS signal
17 that was not dependent on the ion hydrate distribution or the total ion signal.

18 **2.4.4 OH rate constant measurement**

19 A relative rate constant measurement similar to a recent study reported by our laboratory (Jacobs
20 et al., 2013) was performed to measure the 4,3-HNI + OH rate constant. In this method, 4,3-HNI
21 and a competitor with a known rate constant are flowed together through the moveable injector
22 (described in Section 2.4.1) and react with the OH radical in the flow tube. Assuming both
23 compounds react only with OH radicals under the experimental conditions, the two compounds
24 are competing with each other for reaction with OH radicals:



27 The rate laws for 4,3-HNI and the competitor are given by Eqs. 1 and 2, respectively:

1
$$\frac{d[4,3-HNI]}{dt} = k_4[4,3-HNI][OH] \quad (1)$$

2
$$\frac{d[Competitor]}{dt} = k_5[Competitor][OH] \quad (2)$$

3 where k_4 and k_5 are rate constants for Reactions 4 and 5 respectively. By dividing Eq. 1 by Eq. 2
4 and solving the resulting differential equation by separation of variables, it can be shown that:

5
$$\ln \frac{[4,3-HNI]_{t,0}}{[4,3-HNI]_{t,OH}} = \frac{k_4}{k_5} \ln \frac{[Competitor]_{t,0}}{[Competitor]_{t,OH}} \quad (3)$$

6 where $[4,3-HNI]_{t,0}$ and $[competitor]_{t,0}$ are the concentration of 4,3-HNI and the competitor species
7 in the absence of OH radicals at time t , and $[4,3-HNI]_{t,OH}$ and $[competitor]_{t,OH}$ are the
8 concentrations of 4,3-HNI and the competitor species in the presence of OH radicals at time t .
9 The relative depletions of 4,3-HNI and the competitor were monitored when the OH source was
10 turned on and off. From the relative depletions, the 4,3-HNI OH radical rate constant (k_4) was
11 determined by plotting $\ln([4,3-HNI]_{t,0}/[4,3-HNI]_{t,OH})$ vs. $\ln([competitor]_{t,0}/[competitor]_{t,OH})$ and
12 determining the slope (k_4/k_5). Because the competitor's OH radical rate constant (k_5) was known,
13 a value for k_4 was determined.

14 The relative rate measurement does not require knowledge of the absolute concentrations of the
15 epoxide and competitor species (rather, relative concentrations—which are assumed to be
16 proportional to the CIMS signal—are required), nor does it require knowledge of the absolute
17 reaction time (which is a fixed quantity in Eq. 3). Both of these characteristics are important for
18 the present experiments because the vapor pressure (which is needed to calculate the absolute
19 concentrations in the flow tube) of 4,3-HNI is unknown, and the flow tube was operated in the
20 laminar-turbulent flow transition region (Seeley et al., 1993) where a straightforward relationship
21 between bulk flow velocity and molecular velocities does not exist (i.e. time of reaction was not
22 known). By operating the flow system in this transition region, the reaction time was increased
23 and more extensive loss of both 4,3-HNI and the competitor species was observed. Different
24 reaction conditions were obtained by varying the time of reaction (injector distance), 4,3-HNI
25 concentration and competitor concentration. Both 4,3-HNI and the competitors contained
26 hydroxyl groups (which are excellent proton transfer targets) and were detected using PTR-
27 CIMS.

1 To assess the potential existence of systematic error, relative rate measurements for 4,3-HNI were
2 performed using multiple competitors with varying, well-measured OH rate constants. The
3 competitors used were methacrolein, allyl alcohol and 2-methyl-2-propen-1-ol with OH rate
4 constants of 2.9×10^{-11} (Atkinson et al., 2006), 4.9×10^{-11} (Holloway et al., 2005; Orlando et al.,
5 2001; Le Person et al., 2009) and 9.2×10^{-11} (Cometto et al., 2008) $\text{cm}^3 \text{ molecule}^{-1} \text{ s}^{-1}$,
6 respectively. Using a previously described procedure (Jacobs et al., 2013), the relative depletion
7 for each competitor was normalized to the depletion of methacrolein, and all of the data were
8 used to determine a single value for k_4/k_5 .

9 **2.4.5 OH oxidation product study**

10 To explore the mechanism of the OH reaction with 4,3-HNI, a PTR-CIMS-based study of the
11 reaction products was performed. The organic hydroxynitrates were added to the flow system
12 and mass spectra were collected with the OH source on and off. Comparison of these mass
13 spectra revealed which masses corresponded to products of the OH reaction. These masses were
14 quantitatively monitored with the OH source on and off in both low NO_x (no extra NO added)
15 and high NO_x (NO added to $>1 \times 10^{13} \text{ molecules cm}^{-3}$) condition. In the low NO_x experiments,
16 observed products are likely formed from peroxy + peroxy (including hydroperoxy formed from
17 side reactions in the microwave OH radical source) radical interactions, while in the high NO_x
18 experiments, product formation is most likely from peroxy + NO reactions. Assuming equivalent
19 PTR-CIMS response factors (each species contains an OH functional group and previous work as
20 shown that a variety of alcohols possess very similar PTR rate constants (Zhao and Zhang,
21 2004)), the relative product ratios were determined by comparing the signal from one product to
22 the sum of the product signals. From the m/z ratios, chemical structures were assigned, and a
23 mechanism was produced to rationalize the observed products. Different isomeric species with
24 the same m/z ratio cannot be distinguished with this quadrupole-based CIMS instrument;
25 therefore the proposed products are those that are easiest to rationalize in the context of the
26 proposed mechanism and the experimental conditions. For the case of IEPOX formation,
27 synthesized IEPOX was added to the flow system to confirm the IEPOX PTR-CIMS ion
28 distribution in the matrix of the 4,3-HNI oxidation system. The pressure dependence of product
29 formation was investigated by varying the pressure in the flow system from 50-400 Torr by
30 adjusting the inlet to the roughing pump. Due to the pressure-dependent efficiency of the

1 microwave discharge source, measurements could not be performed at pressures greater than 400
2 Torr. At the experimental pressures and timescales, it has also been shown that the flow tube acts
3 as a nearly wall-less reactor (Seeley et al., 1993), which helps to ensure that the measured relative
4 gas phase concentrations are representative of the true relative product yields. Nonetheless, the
5 flow tube was also coated with halocarbon wax to further reduce gas-wall interactions and care
6 was taken to ensure that product signals were fully equilibrated at each point in the measurement.

7 **2.5 Computational Thermodynamics**

8 **2.5.1 Bond dissociation energy**

9 Bond dissociation energies were theoretically determined by calculating the relative energies of
10 the relevant species before and after a homolytic bond cleavage using an adapted version of the
11 G2MS compound method (MG2MS) (Froese et al., 1997), a variation on G2 theory (Curtiss et
12 al., 1991). All calculations were carried out with the Gaussian 03 computational suite (Frisch et
13 al., 2004), and each stationary point was confirmed as an energy minimum by inspecting the
14 calculated frequencies. Geometries of the relevant species were optimized at the B3LYP/6-
15 31G(d,p) level. To calculate the overall energy of the optimized structure, a base energy
16 calculation was performed at the CCSD(T)/6-31G(d) level. In order to correct for basis set
17 effects, a series of additive corrections were performed to simulate a CCSD(T)/6311+G(2df,2p)
18 level calculation. The overall energy expression for the MG2MS scheme is defined as follows:

$$19 \quad E_{\text{MG2MS}} = E_{\text{CCSD(T)/6-31G(d)}} + E_{\text{MP2/6-311+G(2df,2p)}} - E_{\text{MP2/6-31G(d)}} + \text{HLC} \quad (4)$$

20 where HLC is an empirically defined correction term with $\text{HLC} = An_{\alpha} + Bn_{\beta}$ where n_{α} and n_{β} are
21 the number of α - and β - electrons, respectively, and the constants A and B are 6.06 and 0.19 mH,
22 respectively. Previous MG2MS results for atmospherically relevant systems from our lab
23 indicate that the calculated thermodynamic properties are typically accurate to within 2.5 kcal
24 mol^{-1} (Cappa and Elrod, 2001).

25 **2.5.2 IEPOX-4 formation from 4,3-HNI + OH reaction coordinate calculations**

26 The optimized structures and relative energies of the reactants, intermediates and products for
27 IEPOX-4 (*trans* β -IEPOX) formation from 4,3-HNI and BEPOX, a butane-derived epoxide,

1 formation from 1,2-HNB were theoretically determined. In order to achieve convergence, a
2 restricted open shell density functional theory method was used for each single point energy
3 calculation (ROB3LYP/6-31(d)). All calculations were carried out with the Gaussian 03
4 computational suite (Frisch et al., 2004). The frequencies were inspected to ensure each single
5 point calculation was an energy minimum (or had an imaginary frequency for the transition state
6 calculation). Reaction coordinate calculations for the 4,3-HNI mechanism were compared to
7 those from the isoprene-derived hydroperoxide calculations previously published (Paulot et al.,
8 2009b).

10 **3 Results and Discussion**

11 **3.1 NMR assignments**

12 The complete NMR assignments of the synthesized hydroxynitrates are provided in the SI.

13 **3.2 Hydrolysis kinetics of hydroxynitrates**

14 The hydrolysis of the hydroxynitrate isomers was monitored in a variety of acid concentrations (0
15 to 2 M HClO₄), and regardless of the acid concentration, the rate of hydrolysis remained constant.
16 Thus, a general acid catalyzed mechanism (where water protonates the bridging oxygen atom on
17 the nitrate) was assumed to be the predominant hydrolysis mechanism (Whalen, 2005). A
18 standard first order analysis of hydroxynitrate depletion was performed for each hydrolysis
19 reaction. Figure 2 provides a sample plot of $\ln([HNI]/[HNI]_0)$ as a function of time for the
20 reaction of 4,3-HNI in D₂O using the relative integrated areas of the methyl group protons in
21 4,3-HNI and the diol products in ¹H NMR spectra to calculate $[4,3-HNI]/[4,3-HNI]_0$. The slope
22 from this linear regression is equal to -k, the neutral solution hydrolysis rate constant. A similar
23 procedure was used for 1,4-HNI hydrolysis, but (because of product and reactant peak overlap in
24 the methyl region) DSS was added to the reaction mixture and depletion of the hydroxynitrate
25 relative to the peak at 0.00 ppm was monitored. Because of the overlap problem, hydrolysis
26 kinetics of the specific E and Z 1,4-HNI isomers were unable to be distinguished, and a generic
27 1,4-HNI hydrolysis rate was measured.

1 The mechanism and distribution of products observed for 1,4-HNI and 4,3-HNI hydrolysis are
2 given in Figures 3 and 4, respectively. In aqueous solution, 1,4-HNI and 4,3-HNI were found to
3 have first order hydrolysis rate constants of $(6.76 \pm 0.09) \times 10^{-3} \text{ s}^{-1}$ and $(1.59 \pm 0.03) \times 10^{-5} \text{ s}^{-1}$,
4 respectively. These hydrolysis rate constants indicate that the 1,4-HNI and 4,3-HNI lifetimes in
5 neutral solution are 2.46 minutes and 17.5 hours, respectively. The hydrolysis rate constants of
6 similar isoprene-derived, saturated hydroxynitrates have previously been measured in our lab
7 (Darer et al., 2011; Hu et al., 2011). The saturated primary nitrates were found to have lifetimes
8 $>2500 \text{ hr}$, while the saturated tertiary nitrates had lifetimes of a few minutes in neutral solution.
9 Thus the allylic nature of the 1,4-HNI and 4,3-HNI transition states apparently lowers the
10 activation barrier sufficiently to make neutral hydrolysis of the primary and secondary
11 hydroxynitrates occur on a much faster time scale than the previously studied saturated primary
12 and secondary hydroxynitrates of isoprene. This hypothesis was tested by measuring the
13 hydrolysis rate constant for another allylic, non-isoprene derived hydroxynitrate, 1,2-HNB. The
14 hydrolysis rate constant and neutral solution lifetime were $(9.95 \pm 0.30) \times 10^{-6} \text{ s}^{-1}$ and 28 hours,
15 respectively. The hydrolysis reaction for the unsaturated species was again faster than that of
16 similar saturated species, presumably because of the resonance stabilized carbocation.

17 The products were identified using ^1H NMR after the hydrolysis reactions had run to completion
18 (>3 lifetimes). Each of the diol products had been previously prepared in our lab, and NMR
19 spectra of each were available for reference. Quantification of the product distribution was
20 accomplished using the integrated areas of the peaks in the methyl region. Based on the
21 distribution of products, it appears that (as expected) the dominant product for both of the
22 isomers is derived from the more substituted carbocation intermediate. For 1,4-HNI hydrolysis,
23 70% of the product is derived from the tertiary carbocation with the remaining 30% being derived
24 from the primary carbocation. The yields for 4,3-HNI hydrolysis were similar with the secondary
25 carbocation leading to 66% of the total product and the primary carbocation leading to 34% of
26 the total product. The “E” primary carbocation diol was preferred in both cases; it formed 100%
27 of the time for the 1,4-HNI product (even though the initial product was 5:1 E:Z 1,4-HNI), and
28 was preferred in a 3:1 ratio over the Z-isomer for the 4,3-HNI hydrolysis.

1 3.3 Gas phase oxidation of hydroxynitrates

2 While both 4,3-HNI and 1,4-HNI were successfully synthesized, only 4,3-HNI was thermally
3 stable enough for study in our flow tube CIMS system. Presumably because of its fast hydrolysis
4 rate constant and the presence of some water impurity, 1,4-HNI quickly decomposed into both
5 the diol and a more volatile aldehyde. While the aldehyde component represented only a minor
6 fraction of the condensed phase 1,4-HNI sample (as ascertained via ^1H NMR), the very high
7 vapor pressure of the aldehyde led to a gas phase situation in which 1,4-HNI was a minor
8 component.

9 3.3.1 Gas phase OH rate constant of 4,3-HNI

10 The OH rate constant for 4,3-HNI was obtained via competition experiments, using methacrolein,
11 allyl alcohol and 2-methyl-2-propen-1-ol as the competitors with known rate constants. Like 4,3-
12 HNI, all of the competitors were unsaturated alkenols which reacted with OH via an addition
13 mechanism and at the usual 100 torr operating pressure of the flow tube, were all at their high
14 pressure rate constant limit. The signals from the competitors and 4,3-HNI were monitored with
15 the OH source on and off. Because all of the competitors were normalized to methacrolein, all of
16 the data for each competitor were plotted together. The plot of $\ln([4,3\text{-HNI}]_{t,0}/[4,3\text{-HNI}]_{t,\text{OH}})$ vs.
17 $\ln([\text{competitor}]_{t,0}/[\text{competitor}]_{t,\text{OH}})$ is shown in Figure 5. The slope of the best fit line in Figure 5,
18 1.257 ± 0.0058 , is equal to the ratio of 4,3-HNI's OH rate constant to methacrolein's OH rate
19 constant (k_4/k_5). From methacrolein's OH rate constant, $2.9 \pm 0.3 \text{ cm}^3 \text{ molecule}^{-1} \text{ s}^{-1}$ (Atkinson et
20 al., 2006), the 4,3-HNI + OH rate constant was calculated to be $3.64 \pm 0.41 \times 10^{-11} \text{ cm}^3 \text{ molecule}^{-1}$
21 s^{-1} (one standard deviation error, which includes contributions from both the relative rate constant
22 uncertainty in k_4/k_5 and uncertainty in the absolute rate constant of the competitor).

23 A very recent study has reported the OH rate constant with 4,3-HNI and found it to be $(4.2 \pm 0.7) \times$
24 $10^{-11} \text{ cm}^3 \text{ molecule}^{-1} \text{ s}^{-1}$ (Lee et al., 2014). This value is in good agreement with the 4,3-HNI OH
25 rate constant measured in this work and confirms the expectation that the OH rate constant is not
26 pressure dependent between 100 and 760 torr total pressure. The OH rate constant for a similar
27 hydroxynitrate, 2-hydroxy-1-nitrato-but-3-ene (2,1-HNB), was measured separately and found to
28 be $(3.62 \pm 0.72) \times 10^{-11} \text{ cm}^3 \text{ molecule}^{-1} \text{ s}^{-1}$ (Treves and Rudich, 2003). Therefore, it appears that
29 the value of the OH + 4,3-HNI rate is well-constrained by several experimental measurements.

1 3.3.2 4,3-HNI gas phase oxidation product study

2 3.3.2.1 Identification of products

3 Because 4,3-HNI is an unsaturated hydrocarbon, it is expected to react with OH via an addition
4 mechanism forming a hydroxy alkyl radical. The OH radical could add to either of the carbon
5 atoms in the double bond, so there is the potential for multiple, different reaction pathways. As
6 described in the experimental section, the product species were identified by comparing mass
7 spectra taken with the microwave on and off, and then looking for new signals in the “OH
8 source-on” PTR-CIMS spectrum. Because all of the predicted products contained alcohol
9 groups, they were all assumed to have equal PTR-CIMS response factors. This allowed direct
10 comparison of the signals to determine the relative molar product yields.

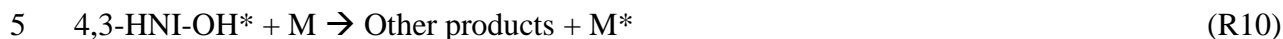
11 Table 2 shows the deduced product structure (based on the $MH^+(H_2O)_n$ signal carriers observed),
12 with the specific isomers rationalized within the context of the overall mechanism. For the cases
13 of C-C bond dissociation reaction types, there are two reaction products. However, due to mass
14 coincidence complications, only one of the products (the product listed in Table 2) was quantified
15 via PTR-CIMS in each case. From the structures of the products, a proposed mechanism for the
16 formation of products from 4,3-HNI was developed (Figure 6). Based on the products observed,
17 it seems likely that the OH radical adds to the double bond almost exclusively at the C1 position.
18 This generates the thermodynamically preferred tertiary radical over the primary radical from C2
19 addition. The alkyl radical can either undergo a unimolecular rearrangement to produce an
20 isoprene epoxide (IEPOX)—either *cis*- or *trans*- β -IEPOX (IEPOX-3 and IEPOX-4,
21 respectively)—and NO_2 , or it can react with O_2 , forming a peroxy radical. The competition
22 between the two reactions was found to be pressure dependent and is discussed below. The
23 peroxy radical can react with either NO (added to the flow system) or HO_2 (a by-product of the
24 microwave discharge source) to generate the alkoxy radical. The C2-C3 bond can fission,
25 generating hydroxyacetone (HAC), glycolaldehyde and NO_2 , or the C1-C2 bond can break,
26 which results in formaldehyde and a methylvinylketone hydroxynitrate (MVKN). The relative
27 yields of the products observed by PTR-CIMS at 50 torr and 760 torr (based the on analysis
28 described below) are given in Table 2.

1 IEPOX was identified as a major product at the lower pressure conditions by its unique PTR-
2 CIMS ion distribution. Previous work in our laboratory investigated the reaction of IEPOX with
3 the OH radical (Jacobs et al., 2013), and thus mass spectra of previously collected IEPOX (as
4 well as a sample of previously synthesized IEPOX) were on hand and aided in the identification
5 of IEPOX. In the previous work, PTR-CIMS of IEPOX had peaks at m/z 101, 137, 155, 219 and
6 237 which represent $(\text{IEPOX})\text{H}^+ - \text{H}_2\text{O}$, $(\text{IEPOX})(\text{H}_2\text{O})\text{H}^+$, $(\text{IEPOX})(\text{H}_2\text{O})_2\text{H}^+$, $(\text{IEPOX})_2\text{H}^+ - \text{H}_2\text{O}$
7 and $(\text{IEPOX})_2\text{H}^+$, respectively. All five of these product peaks were observed in the 4,3-HNI
8 product spectra. To confirm there were no matrix effects at work in the 4,3-HNI product studies,
9 the previously synthesized IEPOX was added downstream of the OH source (where it would not
10 have a chance to react with OH radicals), and all of the peaks attributed to IEPOX increased as
11 expected. Thermodynamic calculations for IEPOX formation from 4,3-HNI were performed and
12 compared to the previously proposed mechanism for IEPOX formation from hydroxy peroxides
13 (Paulot et al., 2009b) to further support the experimental observations.

14 A previous atmospheric chamber study looking at the oxidation of 4,3-HNI by the OH radical has
15 also proposed a reaction mechanism (Lee et al., 2014). The Lee et al. reaction mechanism,
16 derived from experiments performed very near atmospheric pressure, also includes MVKN-
17 forming (C1-C2 bond breaking) and hydroxyacetone-forming (C3-C4 bond breaking) channels
18 with 72% and 10% yields, respectively. Their mechanism also suggests that <18% of 4,3-HNI
19 forms a dinitrate species. Unlike the present work, the Lee et al. mechanism does not include
20 IEPOX formation from 4,3-HNI. Our experimental results show that (at atmospheric pressure)
21 the MVKN forming channel, the hydroxyacetone/ NO_2 forming channel and the IEPOX/ NO_2
22 forming channel account for 70%, 17% and 13% of the total product, yield respectively. Many of
23 the aspects in our mechanism coincide with the mechanism proposed by Lee et al. with the
24 exception of a minor, but significant, IEPOX producing product channel.

25 **3.3.2.2 Product pressure dependence**

26 At higher pressures the relative yield of IEPOX from 4,3-HNI decreased. This observation was
27 explained by assuming that the OH + 4,3-HNI reaction followed a Lindeman-Hinshelwood type
28 mechanism (i.e. the energized OH-4,3-HNI adduct can revert to OH + 4,3-HNI, be de-energized
29 by collision, or go on to form products):



6 where (*) represents a high energy complex. At low pressures (low [M]), Reaction 6 competes
 7 with Reaction 7, and the activated complex can revert back to reactants. Previous research has
 8 shown that isoprene's OH rate constant does not change between 2-6 torr indicating that isoprene
 9 is at its high pressure limit at 2 torr (Chuong and Stevens, 2000). The relatively low threshold for
 10 the high-pressure limit was attributed to the isoprene complex's ability to distribute energy into
 11 many vibrational modes and thus decrease the energy in the critical CO vibration. Because 4,3-
 12 HNI is an even larger molecule than isoprene and has even more vibrational modes, the relative
 13 rate of Reaction 7 as compared to Reaction 8 is expected to be even more insignificant at the
 14 experimental pressures (>50 torr).

15 However, because Reaction 8 is dependent on the number of total gas molecules present (i.e.
 16 pressure), and the rate of IEPOX formation was observed to decrease at higher pressures, it was
 17 assumed that IEPOX was formed from the 4,3-HNI-OH* activated complex. Thus, the alkyl
 18 radical branching point in Figure 6 can be more accurately represented by the two competing
 19 reactions, R9 and R10. The IEPOX and "other products" (OP) rates of formation can then be
 20 defined as follows:

$$21 \quad \frac{d[\text{IEPOX}]}{dt} = k_9[4,3\text{-HNI-OH}^*] \quad (5)$$

$$22 \quad \frac{d[\text{OP}]}{dt} = k_{10}[\text{M}][4,3\text{-HNI-OH}^*] \quad (6)$$

23 where k_9 and k_{10} are the rates of Reactions 9 and 10, respectively. Combining these two
 24 expressions yields an equation for the rate of total product (TP) formation:

$$25 \quad \frac{d[\text{TP}]}{dt} = k_9[4,3\text{-HNI-OH}^*] + k_{10}[\text{M}][4,3\text{-HNI-OH}^*] \quad (7)$$

1 The relative yield of IEPOX can then be expressed as the IEPOX rate of formation (Eq. 6) over
2 the total product rate of formation (Eq. 7):

$$3 \frac{\frac{d[IEPOX]}{dt}}{\frac{d[TP]}{dt}} = \frac{d[IEPOX]}{d[TP]} = \frac{k_9[4,3\text{-HNI-OH}^*]}{k_9[4,3\text{-HNI-OH}^*] + k_{10}[M][4,3\text{-HNI-OH}^*]} = \frac{k_9}{k_9 + k_{10}[M]} \quad (8)$$

4 Taking the reciprocal of Eq. 8 yields an expression that is linearly dependent on [M] (and thus
5 pressure):

$$6 \frac{d[TP]}{d[IEPOX]} = \frac{k_9 + k_{10}[M]}{k_9} \alpha 1 + \frac{k_{10}}{k_9} P \quad (9)$$

7 By plotting the inverse of the relative yield of IEPOX vs. pressure, a linear relationship was
8 determined that was used to estimate the relative yield of IEPOX at atmospheric pressure (Figure
9 7). The slope of the best fit line in Figure 7, $y = [(9.05 \pm 0.73) \times 10^{-3}] P(\text{torr}) + 1.07 \pm 0.17$, was
10 used to estimate the yield of IEPOX from 4,3-HNI at atmospheric pressure presented in Table 2.
11 The relative error from the linear regression propagated into the calculated atmospheric pressure
12 IEPOX relative yield was less than 0.08 (13±1%). When extrapolated to lower pressures (0 torr),
13 the yield of IEPOX is calculated to approach 100%, as predicted by Eq. 9. Taken together, these
14 characteristics of the regression analysis demonstrate that the pressure dependence findings are
15 well described by our model. Over each of the entire measured pressure range (50-400 torr), on
16 average the ratio of MVKN formation to HAC formation was observed to remain constant
17 (4.01±0.98). The yields of these two channels at atmospheric pressure were determined by using
18 this ratio and the calculated relative yield of IEPOX. All of the extrapolated relative yields are
19 given in Table 2.

20 **3.3.3 1,2-HNB gas phase oxidation product study**

21 To assess the feasibility of IEPOX formation from other currently synthetically inaccessible
22 isoprene-derived hydroxynitrates, a gas phase oxidation product study on 1,2-HNB was
23 performed to see if epoxide products were formed. The relative yields of the observed products
24 and a proposed mechanism for the formation of the observed products are provided in Table 3
25 and Figure 8, respectively. The mechanism is similar to that of 4,3-HNI: the OH radical initially
26 adds to carbon 4 creating a secondary alkyl radical. The radical can then undergo unimolecular
27 rearrangement to form a butane epoxide (BEPOX) and NO₂, or it can react with O₂ forming the

1 peroxy radical. The peroxy radical reacts with either NO or HO₂ to create the alkoxy radical.
2 Reaction with O₂ can cause the C3-C4 bond to break resulting in formaldehyde and
3 hydroxynitrate propanal, or the C2-C3 bond can break leading to two equivalents of
4 glycolaldehyde and the release of one NO₂ molecule. The proportion of C3-C4 to C2-C3 bond
5 fragmentation in 1,2-HNB oxidation is roughly the same as the proportion of C1-C2 to C2-C3
6 bond fragmentation in 4,3-HNI oxidation. Thus, 1,2-HNB and 4,3-HNI release roughly the same
7 amount of NO₂ when further oxidized by OH.

8 At higher pressures, the relative epoxide yields were once again observed to decrease. The
9 mechanism for BEPOX formation from 1,2-HNB was assumed to be the same as the mechanism
10 for IEPOX formation from 4,3-HNI, and a pressure dependence product study was performed.
11 Again the inverse of the relative yield of BEPOX was plotted vs. pressure to give a linear
12 relationship (Figure 9). The slope of the best fit line in Figure 9, $y = [(6.80 \pm 0.44) \times 10^{-3}] P(\text{torr})$
13 $+ 0.89 \pm 0.09$, was used to estimate the yield of BEPOX from 1,2-HNB at atmospheric pressure
14 presented in Figure 8. The ratio of C3-C4 bond splitting and C2-C3 bond splitting products was
15 found to be constant, on average, throughout the experiment (5.8 ± 1.6). This ratio (with the
16 calculated relative yield of BEPOX) was used to determine the yields of the fragmentation
17 pathways at atmospheric pressure. The calculated relative yields of the products at atmospheric
18 pressure are presented in Table 3 and Figure 8.

19 The formation of IEPOX from 4,3-HNI and BEPOX from 1,2-HNB suggests that epoxide
20 formation may be a general mechanism that is operative whenever an alkyl radical is adjacent to
21 the nitrate functional group. This finding suggests that other isomers of isoprene-derived
22 hydroxynitrates should be capable of forming IEPOX compounds through OH reaction.

23 **3.4 IEPOX formation thermodynamics calculations**

24 **3.4.1 Bond dissociation energy calculations**

25 To confirm the feasibility of IEPOX (specifically IEPOX-4 or *trans*- β -IEPOX) formation from
26 4,3-HNI, the O-N bond dissociation energy was calculated and compared to the O-O bond
27 dissociation energy for isoprene hydroperoxide (ISOPOOH), the previously proposed IEPOX-
28 4 precursor (Paulot et al., 2009b). The calculations were performed using the adapted G2MS

1 procedure described in the experimental section. The energies of the relevant species were
2 calculated according to Eq. 4, and the bond dissociation energy was determined by finding the
3 difference in energy between the products and reactants after homolytic cleavage of the relevant
4 bond. The O-O and O-N bond dissociation energies for hydrogen peroxide and nitric acid were
5 also calculated, both to validate the MG2MS method and to serve as a point of comparison for
6 the bond dissociation energies for the isoprene derived compounds. The calculated bond
7 dissociation energies are presented in Table 4.

8 The experimental O-O and O-N bond dissociation energies for hydrogen peroxide and nitric acid
9 are 50.4 and 49.3 kcal mol⁻¹, respectively (Lou, 2007). Thus, as found in our previous
10 implementation of the MG2MS method, the calculated values are quite accurate (Cappa et al.
11 2001). The O-N bond dissociation energy for 4,3-HNI is somewhat lower than the O-O bond
12 dissociation energy for ISOPOOH. While this calculation does not rationalize the kinetic
13 feasibility of 4,3-HNI as a precursor to IEPOX-4 formation, it does demonstrate the
14 thermodynamic feasibility of IEPOX-4 formation from either 4,3-HNI or ISOPOOH.

15 **3.4.2 IEPOX-4 formation from 4,3-HNI + OH reaction coordinate calculations**

16 All stationary points in the reaction of 4,3-HNI to IEPOX-4 (*trans*- β -IEPOX) and in the reaction
17 of 1,2-HNB to *trans*-BEPOX were optimized with ROB3LYP/6-31G(d) method. The transition
18 state (TS) between the alkyl radical and the epoxide each had a single imaginary frequency at 635
19 cm⁻¹ and 731 cm⁻¹ for the 4,3-HNI and 1,2-HNB derived species, respectively. As anticipated,
20 this imaginary mode is a vibration along the O-N bond. The single point energies for the 4,3-
21 HNI to IEPOX-4 and 1,2-HNB to *trans*-BEPOX reactions are provided in Table 5, and the
22 reaction coordinate diagram for IEPOX-4 formation is provided in Figure 10. The previous
23 calculations performed to rationalize IEPOX formation from ISOPOOH found that the level of
24 theory and choice of basis sets used did not significantly influence relative energy aspects of the
25 reaction coordinate diagram (Paulot et al., 2009b). However, we found that restricted open shell
26 density functional theory methods were needed to ensure that energy convergence was achieved
27 for all species. To provide a comparison and corroborate our results, single point energy
28 calculations for IEPOX-4 formation from ISOPOOH were repeated using the ROB3LYP/6-
29 31G(d) method. The calculated energies followed the same general trend as previously observed

1 and had an activation energy ($3.6 \text{ kcal mol}^{-1}$) that was in good agreement with the calculations
2 previously performed on this reaction pathway (Paulot et al., 2009b). The single point energies
3 for the ISOPOOH reaction are also listed in Table 5.

4 The pressure dependence study suggests that the majority of IEPOX formation is derived from
5 the activated 4,3-HNI-OH complex, which has the same energy as the initial reactants. Because
6 the energy of this species far exceeds the energy of the transition state, the magnitude of the
7 activation energy is irrelevant, as depicted in Figure 10. However, once the complex is
8 collisionally deactivated and the excess energy is removed, the energies of the reaction barriers
9 become relevant again. The energy barrier between the alkyl radical and the TS was found to be
10 higher ($11.5 \text{ kcal mol}^{-1}$) for the 4,3-HNI pathway than the ISOPOOH pathway. Thus, once
11 deactivated, substantially less IEPOX is expected to be produced from the 4,3-HNI alkyl radical
12 than the ISOPOOH alkyl radical. Additionally, because the 4,3-HNI-derived alkyl radical is
13 larger and contains more vibrational modes than the ISOPOOH-derived alkyl radical, the 4,3-
14 HNI-OH activated complex is expected to be more easily deactivated by collision than the
15 ISOPOOH-OH activated complex. Taken together, these findings are qualitatively consistent
16 with the present findings that IEPOX only accounts for 13% of the total product formed from
17 4,3-HNI oxidation, while the previous work measured a 75% yield from ISOPOOH oxidation at
18 atmospheric pressure (Paulot et al., 2009b).

19 The BEPOX forming pathway had a similar energy barrier ($11.0 \text{ kcal mol}^{-1}$) to that of the 4,3-
20 HNI pathway, and the 1,2-HNB-OH activated complex is expected to be collisionally deactivated
21 in a similar manner to the 4,3-HNI-OH complex. Again this finding is qualitatively consistent
22 with the finding that IEPOX and BEPOX have similar yields at atmospheric pressure (16% for
23 BEPOX compared to the 13% for IEPOX). Because it is certainly possible for IEPOX to also
24 form from the deactivated alkyl radical (as proposed by Paulot et al., 2009b), the atmospheric
25 pressure yields of IEPOX calculated in this study for the 4,3-HNI + OH reaction are lower bound
26 estimates.

27

1 **4 Atmospheric Implications**

2 **4.1 Potential aerosol phase hydrolysis of 4,3-HNI and 1,4-HNI**

3 The 4,3-HNI and E/Z 1,4-HNI isomers have previously been identified as the products of OH-
4 initiated, high-NO_x oxidation of isoprene (Lockwood et al., 2010; Paulot et al., 2009a).
5 Additionally, Rindelaub et al. recently demonstrated that for similar species produced from α-
6 pinene, the aerosol phase partitioning reaction was competitive with the gas phase oxidation
7 processes (Rindelaub et al., 2014). If the Henry's law constants for 4,3-HNI and 1,4-HNI (and
8 other isoprene-derived hydroxynitrates) are large enough, the hydrolysis constants measured in
9 this work indicate that aerosol phase hydrolysis (at all pH values, due to the general acid catalysis
10 mechanism) should be efficient on an atmospherically relevant time scale (<1 day).

11 **4.2 Gas phase OH-initiated oxidation of 4,3-HNI**

12 The experimental determination of a fast OH + 4,3-HNI rate constant confirms the expectation
13 that isoprene hydroxynitrates will have a relatively short atmospheric lifetime (for an average OH
14 concentration of 1×10^6 molecules cm⁻³, the 4,3-HNI lifetime is only 7.6 hours). The observation
15 of NO_x recycling product pathways suggests that the traditional categorization of low- and high-
16 NO_x processes for isoprene is inadequate for the description of the actual, more subtle
17 mechanisms at work in the atmosphere. In addition to the NO_x recycling, the present finding that
18 a “high-NO_x” species, 4,3-HNI, can lead to the important “low-NO_x” species, IEPOX,
19 emphasizes this point. Several studies have shown that IEPOX is an important isoprene
20 intermediate for the formation of species formed in SOA formation (Paulot et al., 2009b; Cole-
21 Filipiak et al., 2010; Darer et al., 2011; Lin et al., 2012; Surratt et al., 2010). Based on the
22 IEPOX and BEPOX forming mechanisms that we have proposed from the OH + 4,3-HNI and
23 OH + 1,2-HNB reactions, respectively, we also expect that the OH reactions with 1,2-HNI and
24 both E/Z 4,1-HNI (Table 1) should also be capable of producing an IEPOX compound. These
25 three hydroxynitrate isomers would go through an intermediate in which the alkyl radical is
26 adjacent to the nitrate group (Figure 11). IEPOX is also possible from E/Z 4,1-HNI, but the OH-
27 initiated oxidation would need to lead to the secondary alkyl radical instead of the
28 thermodynamically preferred tertiary radical. Therefore, IEPOX formation from 1,4-HNI is not

1 likely. Based on the isomer-specific isoprene hydroxynitrate product distributions previously
2 reported (Paulot et al., 2009a), we estimate that 65% of isoprene hydroxynitrates have the ability
3 to form IEPOX. The present findings indicate a potentially greater role for IEPOX even under
4 “high NO_x” atmospheric conditions, which could impact our understanding of both the gas and
5 aerosol phase chemistry of isoprene derived compounds for varying NO_x conditions. Indeed, this
6 newly discovered mechanism may help to explain the previous detection of IEPOX-derived SOA
7 components under high NO_x conditions (Surratt et al., 2010; Budisulistiorini et al., 2013).

8

9 **5 Conclusions**

10 4-hydroxy-3-nitroxy isoprene (4,3-HNI) and E/Z 1-hydroxy-4-nitroxy isoprene (1,4-HNI),
11 representing three of the eight possible isoprene-derived hydroxynitrates, have been synthesized
12 and characterized with NMR. The unimolecular, neutral-solution hydrolysis rate constants for
13 4,3-HNI and the 1,4-HNI isomers (as determined via NMR spectroscopy) were $(1.59 \pm 0.03) \times 10^{-5}$
14 s^{-1} and $(6.76 \pm 0.09) \times 10^{-3} s^{-1}$, respectively. The measured rate constants were unaffected by
15 increasing acid strength (up to 2.0 M HClO₄), thus a general acid catalysis mechanism (where
16 water molecules protonate the bridging oxygen atom) was proposed. The lifetimes of these
17 unsaturated hydroxynitrates (17.5 hours and 2.46 minutes for 4,3-HNI and 1,4-HNI, respectively)
18 are several orders of magnitude smaller than the lifetimes for similar non-tertiary saturated
19 hydroxynitrates.

20 The rate constant for the OH radical initiated oxidation of 4,3-HNI was measured using the FT-
21 CIMS relative rate technique. The OH rate constant was measured to be $(3.64 \pm 0.41) \times 10^{-11} \text{ cm}^3$
22 $\text{molecule}^{-1} \text{ s}^{-1}$. A mechanism for the formation of the observed products (including an IEPOX
23 species) was proposed (Figure 6). Based on estimates of the atmospheric pressure yields of the
24 products, roughly 30% of the NO_x sequestered by 4,3-HNI will be released upon OH reaction.
25 IEPOX, a species important for SOA formation, was observed to be a minor but significant
26 product of 4,3-HNI oxidation. This new IEPOX-forming pathway was supported by
27 computational results that indicate that the reaction mechanism is similar to the established
28 hydroperoxide IEPOX-forming pathway (Paulot et al., 2009b). A similar experimental and
29 computational investigation of the OH reaction with 1-hydroxy-2-nitroxy-3-butene (1,2-HNB)

1 also indicated significant epoxide product formation. Based on these findings, it is expected
2 several of the other isoprene-derived hydroxynitrates, in total, accounting for 65% of all isoprene-
3 derived hydroxynitrates, will also be able to form IEPOX species. The formation of IEPOX (a
4 “low NO_x” compound) from a hydroxynitrate (a “high NO_x” compound) suggests that, as has
5 previously been discussed (Wennberg, 2013), the traditional low- and high-NO_x descriptors are
6 insufficient to explain the more subtle chemical mechanisms at work in the atmosphere.

7

8 **Acknowledgments**

9 This work was supported by the National Science Foundation under Grant No. 1153861.

1 **References**

- 2 Atkinson, R.: Gas-phase tropospheric chemistry of organic compounds: a review, *Atmos.*
3 *Environ.*, 24(1), 1–41, 1990.
- 4 Atkinson, R., Baulch, D. L., Cox, R. A., Crowley, J. N., Hampson, R. F., Hynes, R. G., Jenkin,
5 M. E., Rossi, M. J. and Troe, J.: Evaluated kinetic and photochemical data for atmospheric
6 chemistry: Volume II – gas phase reactions of organic species, *Atmos. Chem. Phys.*, 6, 3625–
7 4055, doi:10.5194/acp-6-3625-2006, 2006.
- 8 Atkinson, R., Baulch, D. L., Cox, R. a., Crowley, J. N., Hampson, R. F., Hynes, R. G., Jenkin, M.
9 E., Rossi, M. J. and Troe, J.: Evaluated kinetic and photochemical data for atmospheric
10 chemistry: Volume III – gas phase reactions of inorganic halogens, *Atmos. Chem. Phys.*, 7, 981–
11 1191, doi:10.5194/acp-7-981-2007, 2007.
- 12 Budisulistiorini, S. H., Canagaratna, M. R., Croteau, P. L., Marth, W. J., Baumann, K., Edgerton,
13 E. S., Shaw, S. L., Knipping, E. M., Worsnop, D. R., Jayne, J. T., Gold, A., and Surratt, J. D.:
14 Real-time continuous characterization of secondary organic aerosol derived from isoprene
15 epoxydiols in downtown Atlanta, Georgia, using the Aerodyne Aerosol Chemical Speciation
16 Monitor, *Environ. Sci. Technol.*, 47, 5686-5694, 10.1021/es400023n, 2013.
- 17 Cappa, C. D. and Elrod, M. J.: A Computational Investigation of the Electron Affinity of CO₃
18 and the Thermodynamic Feasibility of CO₃-(H₂O)_n + ROOH Reactions, *Phys. Chem. Chem.*
19 *Phys.*, 3, 2986–94, 2001.
- 20 Carlton, A. G., Wiedinmyer, C. and Kroll, J. H.: A review of Secondary Organic Aerosol (SOA)
21 formation from isoprene, *Atmos. Chem. Phys. Discuss.*, 9, 8261–8305, doi:10.5194/acpd-9-8261-
22 2009, 2009.
- 23 Chen, X., Hulbert, D. and Shepson, P. B.: Measurement of the organic nitrate yield from OH
24 reaction with isoprene, *J. Geophys. Res.*, 103(D19), 25563–68, doi:10.1029/98JD01483, 1998.
- 25 Chuong, B. and Stevens, P. S.: Kinetic Study of the OH + Isoprene and OH + Ethylene Reactions
26 between 2 and 6 Torr and over the Temperature Range 300 - 423 K, *J. Phys. Chem. A*, 104,
27 5230–5237, 2000.
- 28 Chuong, B. and Stevens, P. S.: Measurements of the kinetics of the OH-initiated oxidation of
29 isoprene, *J. Geophys. Res.*, 107(D13), 4162, doi:10.1029/2001JD000865, 2002.
- 30 Cole-Filipiak, N. C., O'Connor, A. E. and Elrod, M. J.: Kinetics of the hydrolysis of
31 atmospherically relevant isoprene-derived hydroxy epoxides., *Environ. Sci. Technol.*, 44, 6718–
32 23, doi:10.1021/es1019228, 2010.

1 Cometto, P. M., Dalmasso, P. R., Taccone, R. a, Lane, S. I., Oussar, F., Daële, V., Mellouki, A.
2 and Le Bras, G.: Rate coefficients for the reaction of OH with a series of unsaturated alcohols
3 between 263 and 371 K., *J. Phys. Chem. A*, 112(19), 4444–50, doi:10.1021/jp7111186, 2008.

4 Curtiss, L. A., Raghavachari, K., Trucks, G. W. and Pople, J. A.: Gaussian-2 theory for molecular
5 energies of first- and second-row compounds, *J. Chem. Phys.*, 94(11), 7221–30, 1991.

6 Darer, A. I., Cole-Filipiak, N. C., O'Connor, A. E. and Elrod, M. J.: Formation and stability of
7 atmospherically relevant isoprene-derived organosulfates and organonitrates., *Environ. Sci.*
8 *Technol.*, 45, 1895–902, doi:10.1021/es103797z, 2011.

9 Elrod, M. J.: Kinetics study of the aromatic bicyclic peroxy radical + NO reaction: overall rate
10 constant and nitrate product yield measurements., *J. Phys. Chem. A*, 115(28), 8125–30,
11 doi:10.1021/jp204308f, 2011.

12 Fiore, A. M., Horowitz, L. W., Purves, D. W., II, H. L., Evans, M. J., Wang, Y., Li, Q. and
13 Yantosca, R. M.: Evaluating the contribution of changes in isoprene emissions to surface ozone
14 trends over the eastern United States, *J. Geophys. Res.*, 110, D12303,
15 doi:10.1029/2004JD005485, 2005.

16 Frisch, M. J., Trucks, G. W., Schlegel, H. B., Scuseria, G. E., Robb, M. A., Cheeseman, J. R.,
17 Montgomery, Jr., J. A., Vreven, T., Kudin, K. N., Burant, J. C., Millam, J. M., Iyengar, S. S.,
18 Tomasi, J., Barone, V., Mennucci, B., Cossi, M., Scalmani, G., Rega, N., Petersson, G. A.,
19 Nakatsuji, H., Hada, M., Ehara, M., Toyota, K., Fukuda, R., Hasegawa, J., Ishida, M., Nakajima,
20 T., Honda, Y., Kitao, O., Nakai, H., Klene, M., Li, X., Knox, J. E., Hratchian, H. P., Cross, J. B.,
21 Bakken, V., Adamo, C., Jaramillo, J., Gomperts, R., Stratmann, R. E., Yazyev, O., Austin, A. J.,
22 Cammi, R., Pomelli, C., Ochterski, J. W., Ayala, P. Y., Morokuma, K., Voth, G. A., Salvador, P.,
23 Dannenberg, J. J., Zakrzewski, V. G., Dapprich, S., Daniels, A. D., Strain, M. C., Farkas, O.,
24 Malick, D. K., Rabuck, A. D., Raghavachari, K., Foresman, J. B., Ortiz, J. V., Cui, Q., Baboul,
25 A. G., Clifford, S., Cioslowski, J., Stefanov, B. B., Liu, G., Liashenko, A., Piskorz, P.,
26 Komaromi, I., Martin, R. L., Fox, D. J., Keith, T., Al-Laham, M. A., Peng, C. Y., Nanayakkara,
27 A., Challacombe, M., Gill, P. M. W., Johnson, B., Chen, W., Wong, M. W., Gonzalez, C. and
28 Pople, J. A.: *Gaussian 03*., 2004.

29 Froese, R. D. J., Svensson, M. and Morokuma, K.: IMOMO(G2MS): A New High-Level G2-
30 Like Method for Large Molecules and Its Applications to Diels-Alder Reactions, *J. Phys. Chem.*
31 *A*, 101(2), 227–233, 1997.

32 Guenther, A., Karl, T., Harley, P., Wiedinmyer, C., Palmer, P. I. and Geron, C.: Estimates of
33 global terrestrial isoprene emissions using MEGAN (Model of Emissions of Gases and Aerosols
34 from Nature), *Atmos. Chem. Phys. Discuss.*, 6, 3181–3210, doi:10.5194/acpd-6-107-2006, 2006.

35 Holloway, A.-L., Treacy, J., Sidebottom, H., Mellouki, A., Daële, V., Bras, G. Le and Barnes, I.:
36 Rate coefficients for the reactions of OH radicals with the keto/enol tautomers of 2,4-
37 pentanedione and 3-methyl-2,4-pentanedione, allyl alcohol and methyl vinyl ketone using the

- 1 enols and methyl nitrite as photolytic sources of OH, *J. Photochem. Photobiol. A Chem.*, 176,
2 183–190, doi:10.1016/j.jphotochem.2005.08.031, 2005.
- 3 Horowitz, L. W., Fiore, A. M., Milly, G. P., Cohen, R. C., Perring, A., Wooldridge, P. J., Hess, P.
4 G., Emmons, L. K. and Lamarque, J.-F.: Observational constraints on the chemistry of isoprene
5 nitrates over the eastern United States, *J. Geophys. Res.*, 112, D12S08,
6 doi:10.1029/2006JD007747, 2007.
- 7 Hu, K. S., Darer, A. I. and Elrod, M. J.: Thermodynamics and kinetics of the hydrolysis of
8 atmospherically relevant organonitrates and organosulfates, *Atmos. Chem. Phys.*, 11, 8307–8320,
9 doi:10.5194/acp-11-8307-2011, 2011.
- 10 Jacobs, M. I., Darer, a I. and Elrod, M. J.: Rate constants and products of the OH reaction with
11 isoprene-derived epoxides, *Environ. Sci. Technol.*, 47, 12868–12876 [online] Available from:
12 [http://www.scopus.com/inward/record.url?eid=2-s2.0-](http://www.scopus.com/inward/record.url?eid=2-s2.0-84888228233&partnerID=40&md5=dad74a68f73b4856dba9a6d6b799a943)
13 [84888228233&partnerID=40&md5=dad74a68f73b4856dba9a6d6b799a943](http://www.scopus.com/inward/record.url?eid=2-s2.0-84888228233&partnerID=40&md5=dad74a68f73b4856dba9a6d6b799a943), 2013.
- 14 Von Kuhlmann, R., Lawrence, M. G., Pöschl, U. and Crutzen, P. J.: Sensitivities in global scale
15 modeling of isoprene, *Atmos. Chem. Phys.*, 4, 1–17, 2004.
- 16 Lee, L., Teng, A. P., Wennberg, P. O., Crouse, J. D. and Cohen, R. C.: On Rates and
17 Mechanisms of OH and O₃ Reactions with Isoprene-Derived Hydroxy Nitrates., *J. Phys. Chem.*
18 *A*, 118(9), 1622–37, doi:10.1021/jp4107603, 2014.
- 19 Lin, Y.-H., Zhang, Z., Docherty, K. S., Zhang, H., Budisulistiorini, S. H., Rubitschun, C. L.,
20 Shaw, S. L., Knipping, E. M., Edgerton, E. S., Kleindienst, T. E., Gold, A. and Surratt, J. D.:
21 Isoprene epoxydiols as precursors to secondary organic aerosol formation: acid-catalyzed
22 reactive uptake studies with authentic compounds., *Environ. Sci. Technol.*, 46, 250–8,
23 doi:10.1021/es202554c, 2012.
- 24 Lockwood, A. L., Shepson, P. B., Fiddler, M. N. and Alaghmand, M.: Isoprene nitrates:
25 preparation, separation, identification, yields, and atmospheric chemistry, *Atmos. Chem. Phys.*,
26 10, 6169–6178, doi:10.5194/acp-10-6169-2010, 2010.
- 27 Lou, Y. R.: *Comprehensive Handbook of Chemical Bond Energies*, CRC Press, Boca Raton, FL.,
28 2007.
- 29 Orlando, J. J., Tyndall, G. S. and Ceazan, N.: Rate Coefficients and Product Yields from
30 Reaction of OH with 1-Penten-3-ol, (Z)-2-Penten-1-ol, and Allyl Alcohol (2-Propen-1-ol), *J.*
31 *Phys. Chem. A*, 105(14), 3564–3569, doi:10.1021/jp0041712, 2001.
- 32 Patchen, A. K., Pennino, M. J., Kiep, A. C. and Elrod, M. J.: Direct Kinetics Study of the
33 Product-Forming Channels of the Reaction of Hydroxyperoxy Radicals with NO, *Int. J. Chem.*
34 *Kinet.*, 39, 353–361, doi:10.1002/kin, 2007.

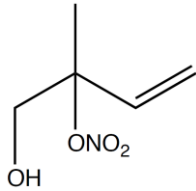
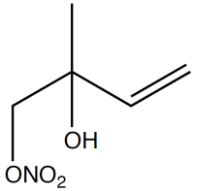
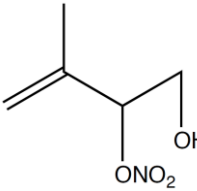
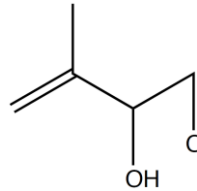
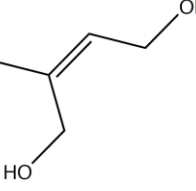
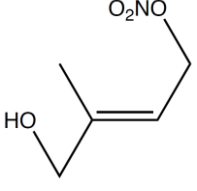
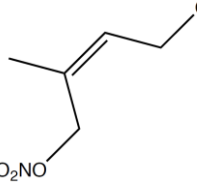
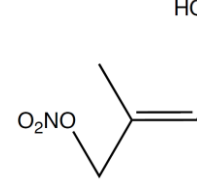
- 1 Paulot, F., Crouse, J. D., Kjaergaard, H. G., Kroll, J. H., Seinfeld, J. H. and Wennberg, P. O.:
2 and Physics Isoprene photooxidation : new insights into the production of acids and organic
3 nitrates, *Atmos. Chem. Phys.*, 9, 1479–1501, 2009a.
- 4 Paulot, F., Crouse, J. D., Kjaergaard, H. G., Kürten, A., St Clair, J. M., Seinfeld, J. H. and
5 Wennberg, P. O.: Unexpected epoxide formation in the gas-phase photooxidation of isoprene.,
6 *Science*, 325(5941), 730–3, doi:10.1126/science.1172910, 2009b.
- 7 Paulot, F., Henze, D. K. and Wennberg, P. O.: Impact of the isoprene photochemical cascade on
8 tropical ozone, *Atmos. Chem. Phys.*, 12, 1307–1325, doi:10.5194/acp-12-1307-2012, 2012.
- 9 Le Person, A., Solignac, G., Oussar, F., Daële, V., Mellouki, A., Winterhalter, R. and Moortgat,
10 G. K.: Gas phase reaction of allyl alcohol (2-propen-1-ol) with OH radicals and ozone, *Phys.*
11 *Chem. Chem. Phys.*, 11, 7619–28, doi:10.1039/b905776e, 2009.
- 12 Rindelaub, J. D., McAvey, K. M. and Shepson, P. B.: Determination of α -pinene-derived organic
13 nitrate yields: particle phase partitioning and hydrolysis, *Atmos. Chem. Phys. Discuss.*, 14, 3301–
14 3335, doi:10.5194/acpd-14-3301-2014, 2014.
- 15 Rollins, A. W., Pusede, S., Wooldridge, P., Min, K. E., Gentner, D. R., Goldstein, a. H., Liu, S.,
16 Day, D. a., Russell, L. M., Rubitschun, C. L., Surratt, J. D. and Cohen, R. C.: Gas/particle
17 partitioning of total alkyl nitrates observed with TD-LIF in Bakersfield, *J. Geophys. Res. Atmos.*,
18 118, 6651–6662, doi:10.1002/jgrd.50522, 2013.
- 19 Seeley, J. V., Jayne, J. T., and Molina, M. J.: High pressure fast-flow technique for gas phase
20 kinetics studies, *Int. J. Chem. Kinet.*, 25, 571-594, 1993.
- 21 Sprengnether, M., Demerjian, K. L., Donahue, N. M. and Anderson, J. G.: Product analysis of the
22 OH oxidation of isoprene and 1, 3-butadiene in the presence of NO, *J. Geophys. Res.*, 107(D15),
23 4268, doi:10.1029/2001JD000716, 2002.
- 24 Surratt, J. D., Chan, A. W. H., Eddingsaas, N. C., Chan, M., Loza, C. L., Kwan, A. J., Hersey, S.
25 P., Flagan, R. C., Wennberg, P. O. and Seinfeld, J. H.: Reactive intermediates revealed in
26 secondary organic aerosol formation from isoprene., *Proc. Natl. Acad. Sci. U. S. A.*, 107(15),
27 6640–5, doi:10.1073/pnas.0911114107, 2010.
- 28 Treves, K. and Rudich, Y.: The Atmospheric Fate of C3 - C6 Hydroxyalkyl Nitrates, *J. Phys.*
29 *Chem. A*, 107, 7809–7817, 2003.
- 30 Wennberg, P. O.: Let's abandon the “high NOX” and “low NOX” terminology, *IGAC News*,
31 50(July 2013), 3–4, 2013.
- 32 Whalen, D. L.: Mechanisms of Hydrolysis and Rearrangement of Epoxides, in *Advances in*
33 *Physical Organic Chemistry*, Volume 40, edited by J. P. Richards, pp. 247–97, Academic Press,
34 London., 2005.

1 Zhao, J., and Zhang, R.: Proton transfer reaction rate constants between hydronium ion (H₃O⁺)
2 and volatile organic compounds, *Atmos. Environ.*, 38, 2177-2185,
3 10.1016/j.atmosenv.2004.01.019, 2004.

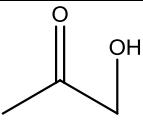
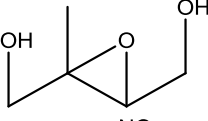
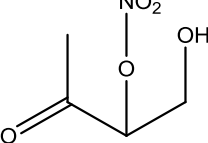
4

5

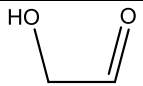
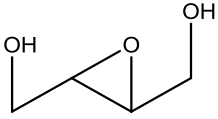
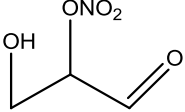
1
2

Structure				
Abbreviation	1,2-HNI	2,1-HNI	4,3-HNI	3,4-HNI
Yield (%)	23.1	1.1	12.8	2.8
Structure				
Abbreviation	(Z)-1,4-HNI	(E)-1,4-HNI	(Z)-4,1-HNI	(E)-4,1-HNI
Yield (%)	4.6	26.5	4.4	24.8

3 **Table 1.** Isoprene-derived hydroxynitrate isomers with their calculated yields (Paulot et al.,
4 2009a).

m/z (MH ⁺)	Deduced molecular species	Relative yield 50 torr (%)	Relative yield 760 torr (%)
75		10	17
119		71	13
150		19	70

1
2 **Table 2.** Relative product yields for 4,3-HNI oxidation at 50 torr (experimental) and 760 torr
3 (calculated).

m/z (MH ⁺)	Deduced molecular species	Relative yield 50 torr (%)	Relative yield 760 torr (%)
61		3	12
105		86	16
136		11	71

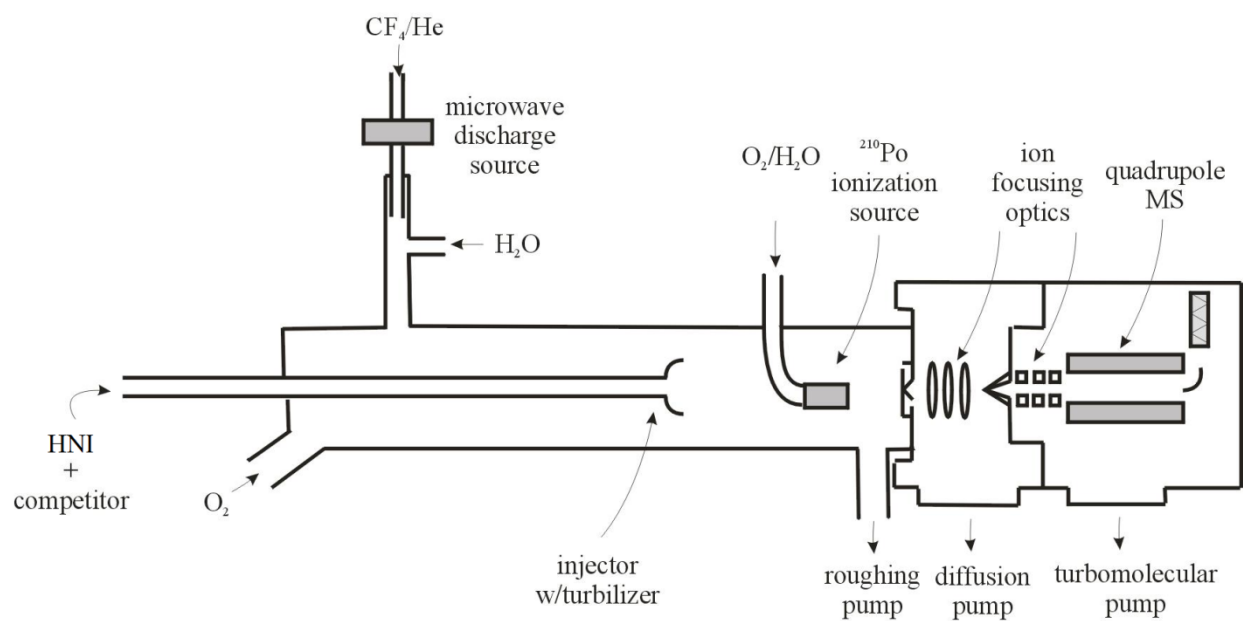
1 **Table 3.** Relative product yields for 1,2-HNB oxidation at 50 torr (experimental) and 760 torr
2 (calculated).

Bond	O-N (4,3-HNI)	O-N (HONO ₂)	O-O (ISOPOOH)	O-O (H ₂ O ₂)
D ₀ (kcal mol ⁻¹)	40.6	49.6	43.8	49.9

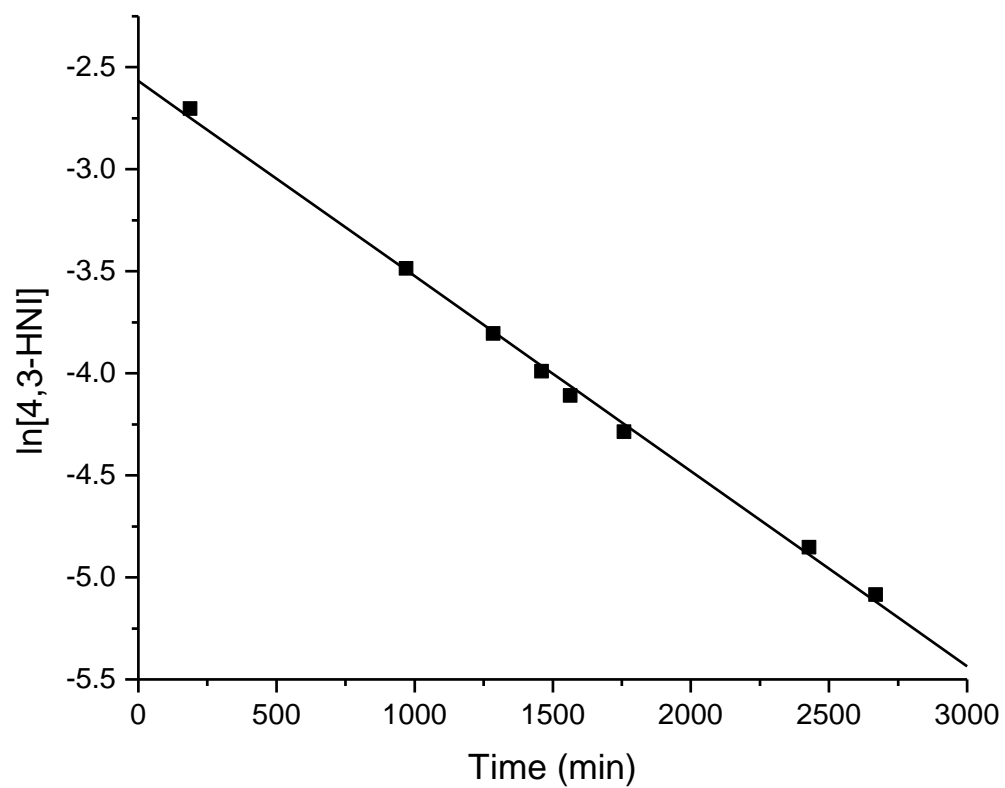
1 **Table 4.** Calculated 0 K bond dissociation energies (D₀) for the relevant species.

Species	4,3-HNI	1,2-HNB	ISOPOOH
Reactant	0	0	0
Alkyl Radical	-36.7	-32.5	-33.0
Transition State	-25.2	-21.5	-29.4
Epoxide Product	-51.0	-53.3	-42.5

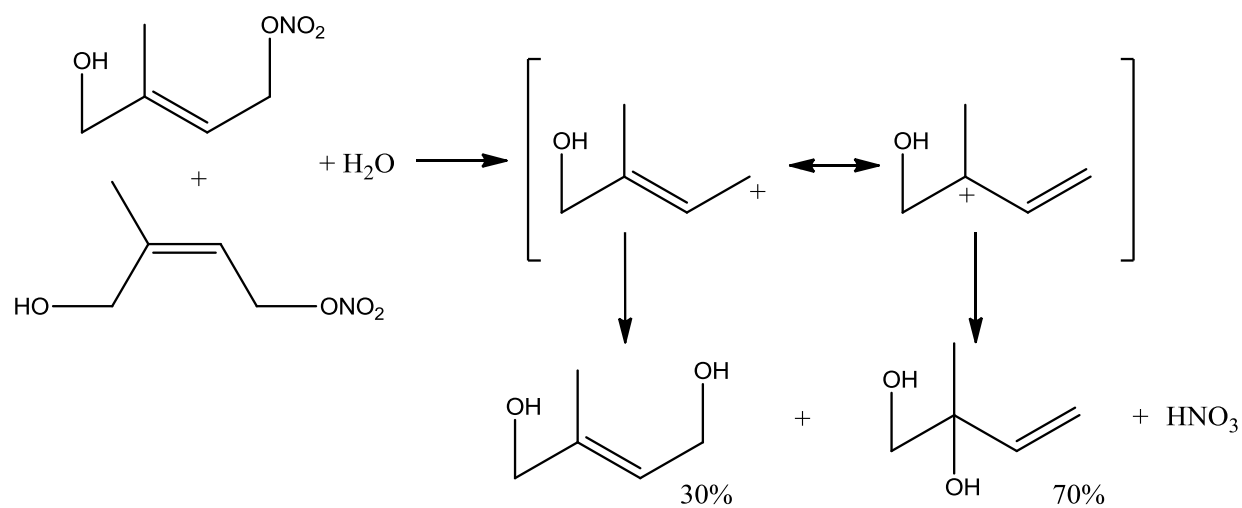
1 **Table 5.** Calculated relative energies (kcal/mol) of the stationary points in the reactant + OH →
2 epoxide + NO₂ reaction. All energies were calculated using the ROB3LYP/6-31G(d) method.



1
 2 **Fig. 1.** Schematic of the FT-CIMS apparatus. The experimental setup in this diagram shows a
 3 relative rate experiment using the $\text{F} + \text{H}_2\text{O}$ OH radical source.

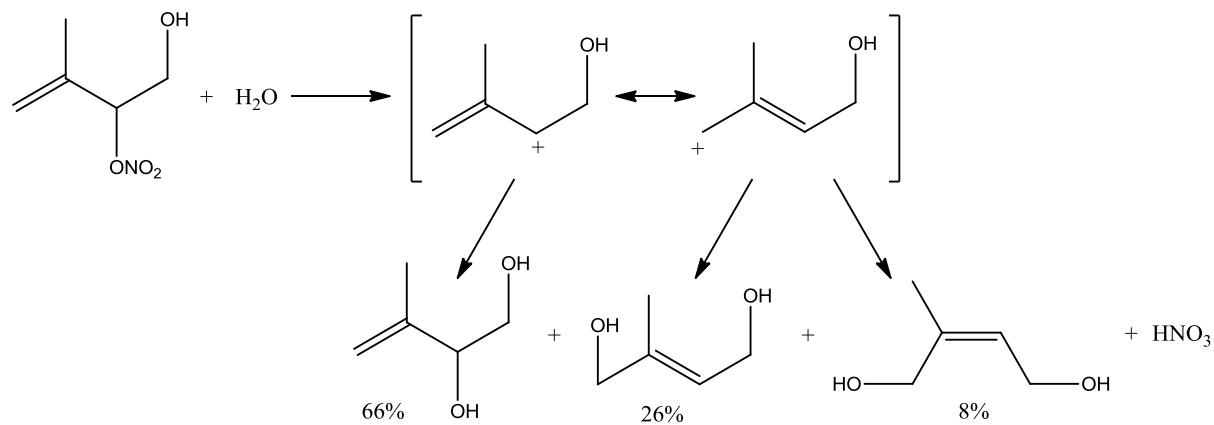


1
2 **Fig. 2.** Sample first-order reactant kinetics plot for the hydrolysis of 4,3-HNI under (initially)
3 neutral D_2O conditions.



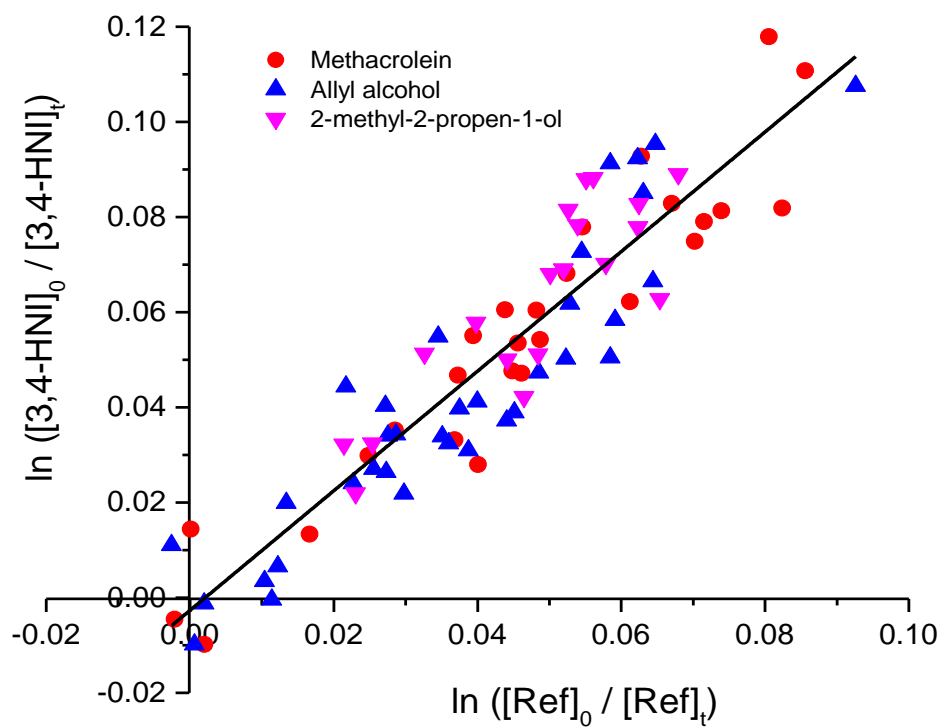
1
2 **Fig. 3.** Mechanism for 1,4-HNI hydrolysis with the distribution of products observed.

1

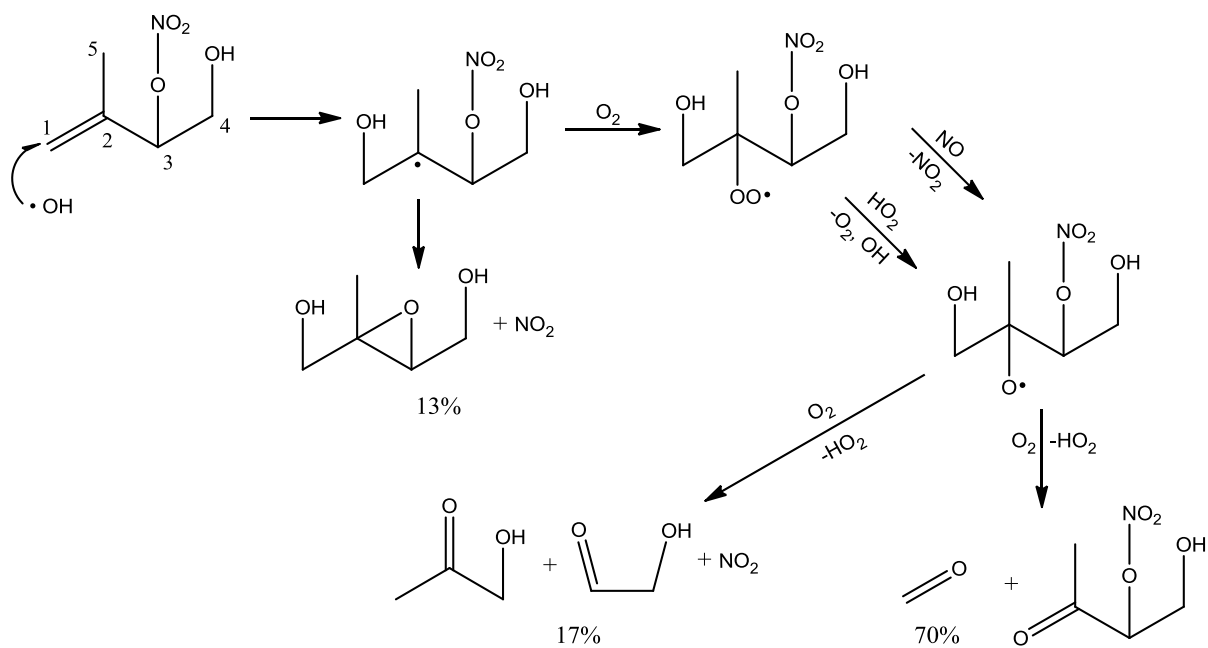


3

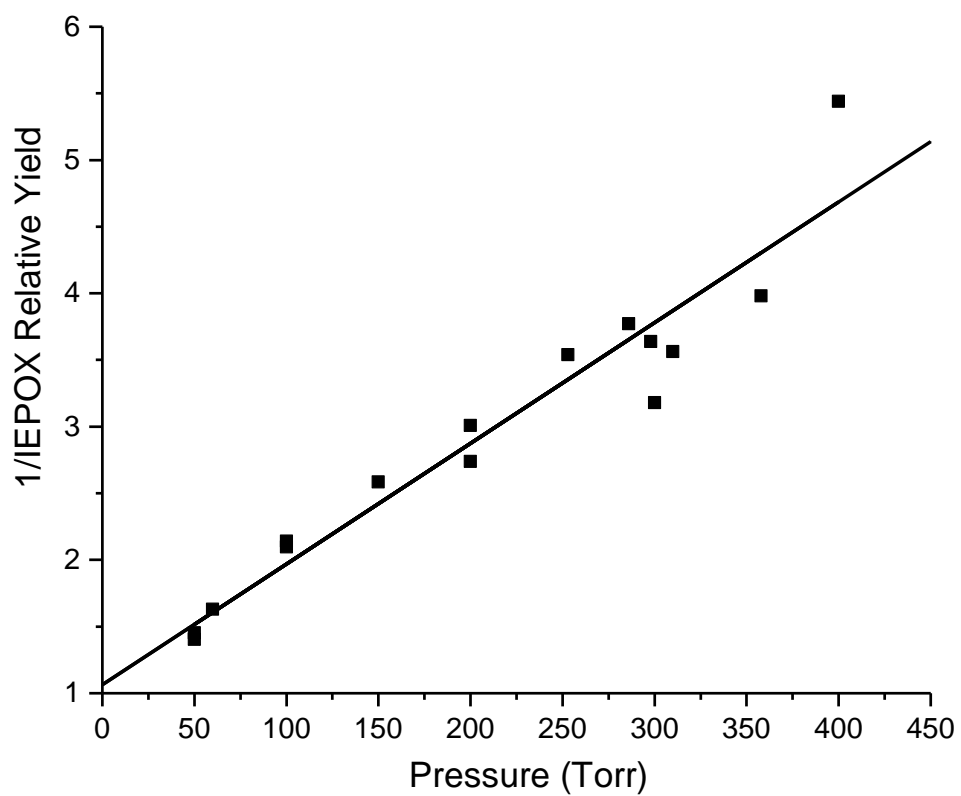
Fig. 4. Mechanism for 4,3-HNI hydrolysis with the distribution of products observed.



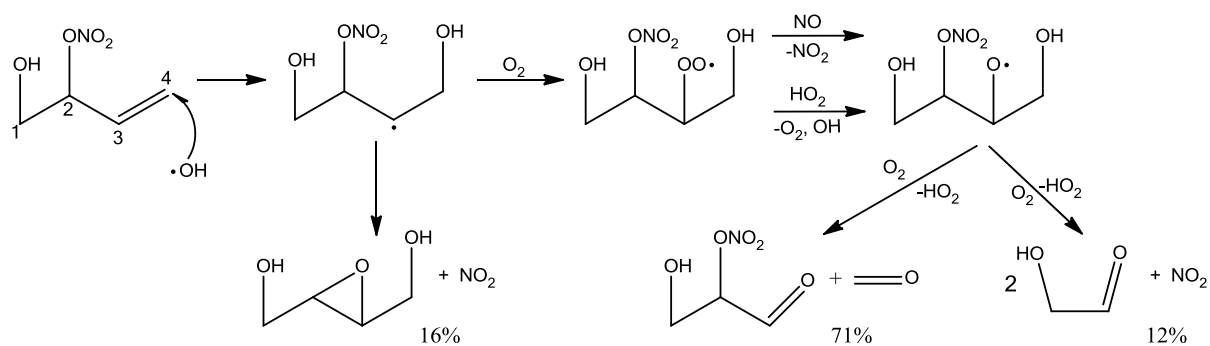
1
2 **Fig. 5.** Relative rate constant determination for 4,3-HNI.



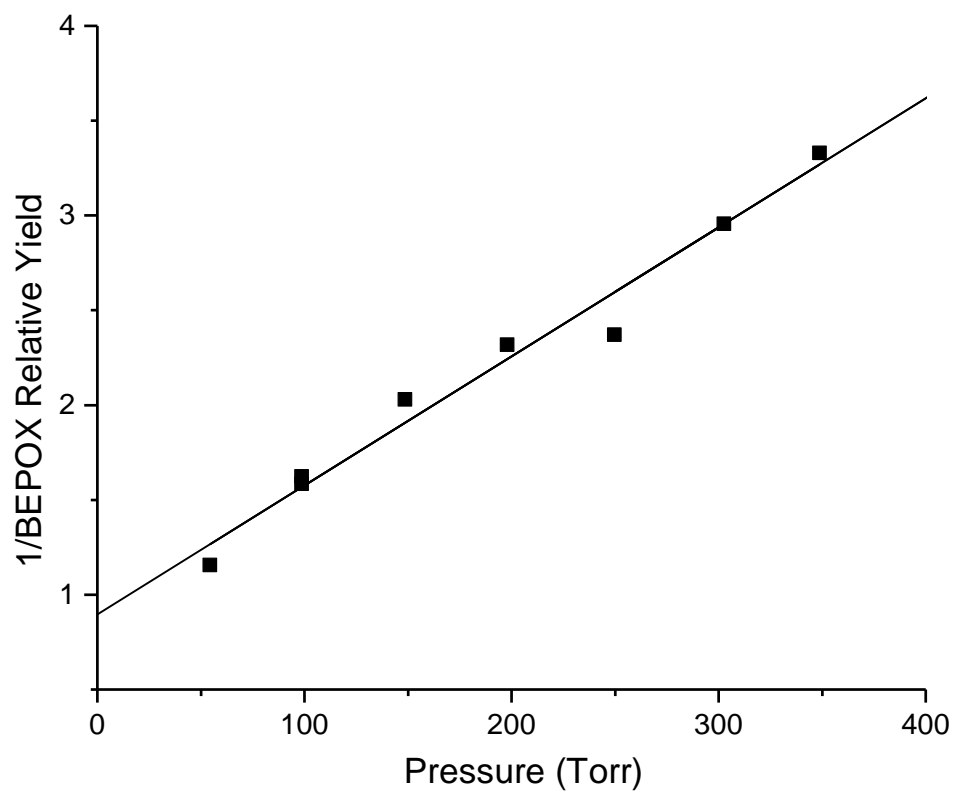
1
 2 **Fig. 6.** Gas phase OH-initiated oxidation mechanism for 4,3-HNI (calculated 760 torr relative
 3 yields are given).



1
2 **Fig. 7.** Pressure dependence of the inverse relative IEPOX yield from 4,3-HNI.

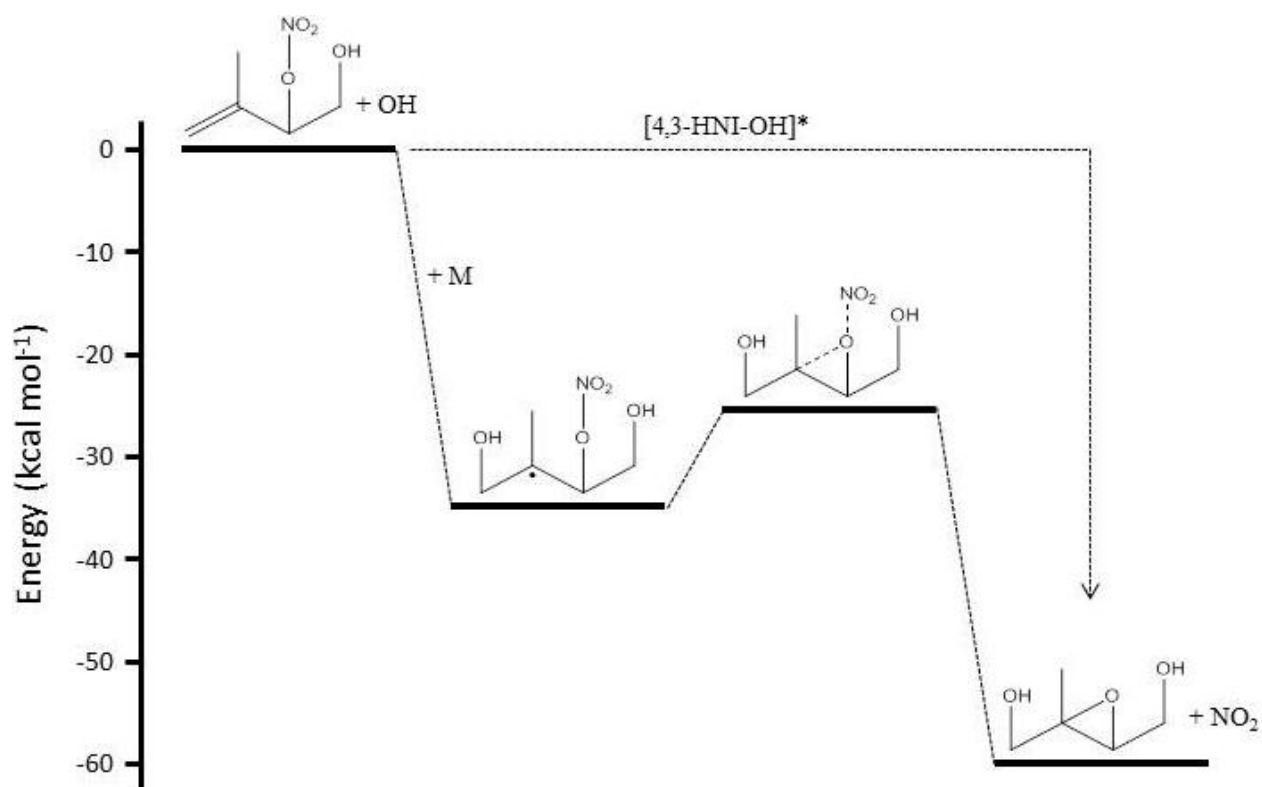


1
 2 **Fig. 8.** Gas phase OH-initiated oxidation mechanism for 1,2-HNB (calculated 760 torr relative
 3 yields are provided).

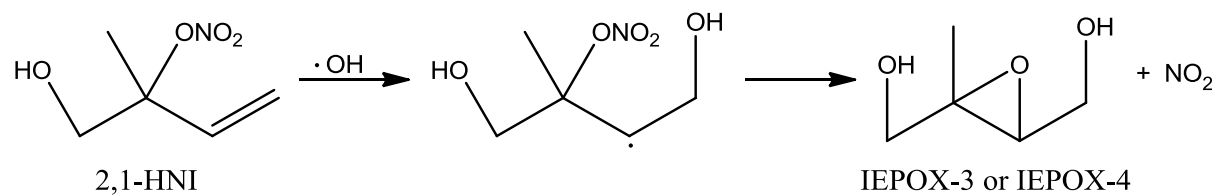
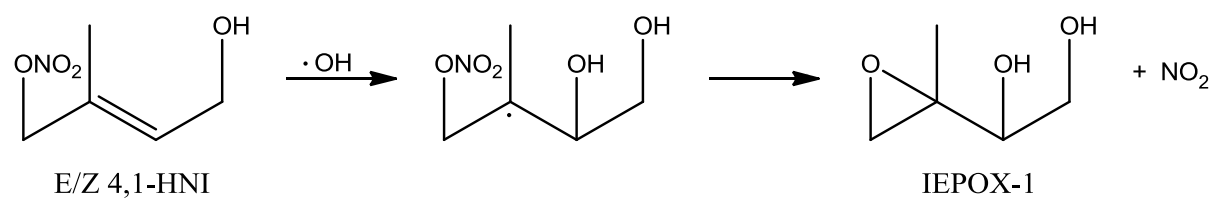


1

2 **Fig. 9.** Pressure dependence of the inverse relative BEPOX yield from 1,2-HNB.



1
 2 **Fig. 10.** Relative energies for the formation of trans-IEPOX from 4,3-HNI. The activated alkyl
 3 radical (4,3-HNI-OH*) resulting from the addition of OH onto the 4,3-HNI double bond is
 4 formed with enough excess energy that it can decompose into IEPOX + NO₂ via the transition
 5 state. Only after being collisionally deactivated by another molecule (M) does the activation
 6 barrier to the TS become relevant. Energies calculated with the ROB3LYP/6-31G(d) method.



1
2
3 **Fig. 11.** Proposed mechanism for IEPOX formation from 4,1-HNI and 2,1-HNI. For both
4 hydroxynitrate isomers, the thermodynamically favored alkyl radical is adjacent to the nitrate
5 group, potentially leading to IEPOX formation.